J. Fluid Mech. (1989), *vol.* 207, *pp.* 489–504
Printed in Great Britain

Buoyant laminar flow of air in a long, square-section cavity aligned with the ambient temperature gradient

By G. S. H. LOCK AND J.-C. HAN
Department of Mechanical Engineering, University of Alberta, Edmonton, Alberta, Canada

(Received 2 June 1988 and in revised form 13 April 1989)

Numerical solutions have been obtained for three-dimensional buoyant flow of air under laminar conditions in a slender, square-section cavity lying parallel to the gradient vector of the temperature field in which it is embedded. Velocity and temperature profiles in the cavity are presented in support of a flow model in which primary and secondary circulation are reconciled by an advective mechanism in the central region. The effect of the temperature gradient, represented by a Rayleigh number, is explored when the cavity is horizontal. The effect of inclining the cavity above and below this horizontal position is also explored. Comparisons are made with related work on cylindrical and two-dimensional rectangular cavities.

1. Introduction

It is known that natural convection inside a slender cavity oriented parallel to the temperature gradient of the material within which it is embedded may create heat transfer rates much greater than if the cavity were completely filled with the embedding material. When the ambient temperature gradient lies parallel to the body force field, either of two situations commonly arises: if the field acceleration opposes the temperature gradient vector, stable stratification occurs; if they are in the same direction and have the same sense, stratification is limited to very small temperature gradients, if it occurs at all. As the temperature gradient (together with the cavity) is rotated relative to the field acceleration the strength of the resulting buoyant circulation varies according to the angular displacement. In a uniform gravitational field this angular displacement is obviously the inclination, here measured in relation to the horizontal position.

Because of its importance to the understanding of convection in thermosyphons, thermal insulation, metal casting and crystallization phenomena, the problem of buoyant circulation in a slender cavity has received much attention. For cavities in which the principal temperature difference $\Delta T = T_H - T_C$ lies parallel to the long axis, length L, the work of Cormack, Leal & Imberger (1974*a*), Cormack, Leal & Seinfield (1974*b*) and Imberger (1974) provides an appropriate point of departure. These were analytic, numerical and experimental studies of a two-dimensional rectangular cavity with the shorter endwalls, length D, being held at different temperatures. Given that the longer walls were horizontal and adiabatic, the flow considered was understandably weak but the authors were able to reveal the characteristic structure found within slender cavities: a central core region of essentially parallel flow joining two end regions of limited extent. The findings were supported later by the analysis of Bejan & Tien (1978*a*).

Ostrach, Loka & Kumar (1980) report some experimental results which extend the above observations on two-dimensional cavities to higher Rayleigh numbers ($Ra = \beta g \Delta T D^3/\nu\kappa$) and lower slenderness ratios ($S = L/D$) for which boundary layer effects become more important. They found that the existence of a parallel core region typically requires slenderness ratios greater than 10:1, although it is also limited to lower Rayleigh numbers, as might be expected. Secondary cells were discovered in the end regions for slenderness ratios less than 5:1, again depending on the Rayleigh number. These results were obtained with non-adiabatic horizontal walls, as distinct from the adiabatic walls employed by Bejan, Al-Homoud & Imberger (1981) in a similar set of experiments which revealed weak secondary circulation in the central region for Rayleigh numbers as high as 1.7×10^7. The latter authors suggested the following regimes: $Ra = O(1)$ divides a pure (horizontal) conduction regime from one in which advection is important; $Ra = O(Pr^2)$, where Pr is the Prandtl number, marks the onset of boundary-layer flow in the end regions; and $Ra = O(S^4)$ marks the onset of non-parallel flow in the central region. More recently, detailed measurements of the temperature and velocity fields in water-filled cavities with adiabatic long walls have been made by Simpkins & Chen (1986) who appear to throw some doubt on the aforementioned location of the parallel/non-parallel transition in the core. Their heat transfer data were found to be in good agreement with the numerical results of Blythe, Daniels & Simpkins (1983).

Buoyant circulation in horizontal cylindrical cavities has also been studied extensively, but largely for situations in which azimuthal variations in wall temperature create a primary flow in a plane normal to the tube axis. Cylinders heated from the side or from below have both been considered. In reviewing twenty years of study, Ostrach (1972) noted the complexity of primary and secondary flow patterns covering a wide range of Rayleigh numbers. Of particular importance here are the alterations in circulation produced by rotation of the ambient temperature gradient relative to the horizontal (see Menold & Ostrach 1965; Sabzevari & Ostrach 1966).

Even more relevant to the present work are the recent studies by Bontoux and coworkers. For a horizontal cylinder with an azimuthally uniform wall temperature varying linearly over its length, Bontoux *et al.* (1986*a*) have systematically organized previous results, notably those of Smutek *et al.* (1985), Schiroky & Rosenberger (1984) and Bejan & Tien (1978*a*, *b*), to emphasize the inherently three-dimensional character of the flow. A finite-difference solution of this problem has been developed by Bontoux *et al.* (1986*c*) who illustrated the structure of the flow with $S = 5$. In particular, they were able to reconcile the longitudinal primary circulation, driven by the difference in end-wall temperatures, with the lateral secondary circulation, driven by radial temperature gradients. The low-Rayleigh-number 'core-driven' regime and the higher-Rayleigh-number 'boundary-layer-driven' regime were again discussed, with the transitional point apparently being located in the vicinity of $Ra = O\ (2.32 \times 10^4)$, based on the cylinder diameter.

The flow regimes for buoyant, laminar circulation in a vertical, cylindrical cavity were first delineated by Lighthill (1953) and later confirmed by Bayley & Lock (1965) for conditions under which the lower part of the cavity was heated and the upper part cooled, i.e. with the gravitational and temperature gradient vectors aligned in the same direction and sense. In attempting to reconcile the opposing flows of the upper and lower halves Bayley & Lock suggested an advective exchange mechanism which enabled hot and cold streams to pass through each other in an hypothetical interdigitative fashion. This mechanism was later confirmed by Japikse & Winter

(1971) who also explored the effect of inclining the cylinder axis with respect to the vertical. Inclination introduces a lateral component of the gravitational acceleration and thus creates a secondary flow which is, however, antisymmetric about the central lateral plane. Although their visual observations were limited to small inclinations from the vertical, Japikse & Winter noted that a strong primary loop, much like that later revealed by Bontoux, soon established itself.

Very recent experiments by Lock & Kirchner (1988) on inclined tubes filled with water have revealed that the Nusselt number exhibits a maximum between the vertical and horizontal positions. In an attempt to explain this behaviour they suggested a flow model in which the antisymmetric secondary flows may be reconciled with the longitudinal primary flow in such a way as to incorporate advective exchange in the vicinity of the central lateral plane, consistent with the visual observations of Japikse & Winter. The present work is a numerical study of this system cast in the form of an inclined, air-filled, square-section tube lying parallel to the ambient temperature gradient. One of its purposes is to test the validity of the model, in detail, when applied to a tube with a slenderness ration of 5:1 inclined at various angles above and below the horizontal position.

2. Formulation

The rectangular coordinate system and principal dimensions used in the description of the cavity are shown in figure 1. The gravitational acceleration g acts along the vertical GO which is always contained in the plane of the axes OX and OZ. Inclination to any degree α is thus effected by rotation about the axis OY. As indicated, the cavity has a length L, breadth B and depth D, the last two of which will be taken equal in this study. Fluid velocities in the X-, Y- and Z-directions are U, V and W, respectively. At any particular value of X, the temperature around the surface of the cavity is taken to be uniform, but its magnitude decreases linearly with X. Thus, with the hotter end of the cavity always contained in the (Y, Z)-plane, the ambient temperature gradient vector rotates with α such that it points in the same direction as the gravitational acceleration only when the cavity is vertical and heated from below. This study will be limited to $-255° \leqslant \alpha \leqslant 75°$ and is therefore not concerned with circulation in the near-vertical position; fluid motion ceases at $\alpha = -90°$, about which position the behaviour of the system varies symmetrically.

The governing equations are those of continuity, motion and energy expressed in the rectangular coordinate system of figure 1. Over a wide range of inclinations and Rayleigh numbers it is unlikely that a single set of non-dimensional variables would normalize the entire set of equations. Accordingly, the choice of each of the length, velocity and pressure scales has been based on the geometry of the cavity and the presumed balance between the inertial, pressure and buoyancy terms in the longitudinal equation of motion. Thus, by defining

$$x = X/L, \quad y = Y/D, \quad z = Z/D, \quad u = U/[\tfrac{1}{2}\beta g(T_H - T_C)\,L]^{\frac{1}{2}},$$
$$v = VL/D[\tfrac{1}{2}\beta g(T_H - T_C)\,L]^{\frac{1}{2}}, \quad w = WL/D[\tfrac{1}{2}\beta g(T_H - T_C)\,L]^{\frac{1}{2}}.$$

and $p = 2P/\beta g\rho(T_H - T_C)L$, where P is the absolute pressure, β is the thermal expansion coefficient and ρ its density, together with

$$\phi = \frac{T - \frac{1}{2}(T_H + T_C)}{\frac{1}{2}(T_H - T_C)},$$

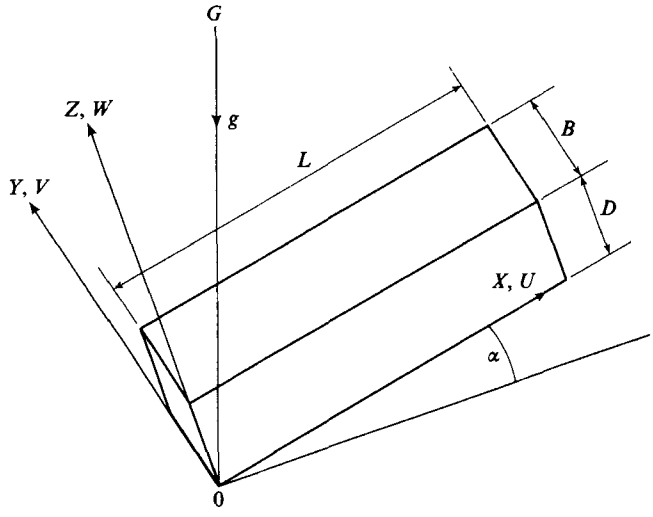

FIGURE 1. Coordinate system.

where T_H, T_C are the endwall temperatures at the hot and cold ends, respectively, the governing equations for steady, laminar flow† may be expressed as

$$\left.\begin{aligned} uu_x+vu_y+wu_z &= -p_x+\phi\sin\alpha+C(u_{xx}+S^2u_{yy}+S^2u_{zz}),\\ uv_x+vv_y+wv_z &= -S^2p_y+C(v_{xx}+S^2v_{yy}+S^2v_{zz}),\\ uw_x+vw_y+ww_z &= -S^2p_z+\frac{\phi\cos\alpha}{S}+C(w_{xx}+S^2w_{yy}+S^2w_{zz}),\\ u_x+v_y+w_z &= 0,\\ u\phi_x+v\phi_y+w\phi_z &= \frac{C}{Pr}(\phi_{xx}+S^2\phi_{yy}+S^2\phi_{zz}), \end{aligned}\right\} \tag{1}$$

in which $C=(2Pr/Ra)^{\frac{1}{2}}$. This study will be limited to air with $Pr=0.71$.

Equations (1) are to be solved subject to the following boundary conditions:

$$\left.\begin{aligned} x=0,1: &\quad \phi=1,-1 \quad \text{for all } y,z,\\ y=0,1: &\quad \phi=1-2x \quad \text{for all } z,\\ z=0,1: &\quad \phi=1-2x \quad \text{for all } y, \end{aligned}\right\} \tag{2}$$

and $u=v=w=0$ over all six boundary planes. The effect of replacing the Dirichlet thermal conditions at the ends with adiabatic conditions will be considered later.

The numerical scheme employed closely follows the SIMPLE-C algorithm (see Patankar 1981; Van Doormaal & Raithby 1984) which has been widely used in the study of both forced and natural convection. The linking of pressure correction and continuity in this method does not lend itself to easy diagnosis, but by limiting the Péclet number and exercising judicious control over relaxation factors the solutions could be made to converge fairly rapidly. Convergence demanded successive agreement within 1% for each of the dependent variables, though the agreement was often much better, typically of the order of 0.1%. As expected, the number of

† The Boussinesq approximation has been used and viscous dissipation has been ignored.

iterations varied with the initial fields, the magnitudes of the principal parameters and, of course, the number of nodes in the finite-difference network. Runs were undertaken with a constant-mesh, $15 \times 15 \times 71$ network, and this served to establish the general flow pattern with reasonable accuracy. Given the observations of Bontoux *et al.* (1986*c*) on the ability of a coarse mesh to represent three-dimensional circulation in a circular cylinder with the same slenderness ratio of 5:1, this mesh is considered adequate for the study of primary and secondary flow in a square cavity.

3. Discussion of results

3.1. *The horizontal cavity*

In the horizontal position, the cavity is well suited for comparison with previous work. The Nusselt number Nu for this position is shown in figure 2 plotted against the Rayleigh number Ra; the slenderness ratio is equal to 5:1. For the thermal boundary conditions stipulated in the previous section, it is possible to define the heat transfer rate, and the corresponding Nusselt number, in several ways. In figure 2 the total heat transfer rate $\dot{Q}$ into, through, and out of, the cavity has been used, regardless of which surfaces or partial surfaces were involved. This was obtained by integrating the normal temperature gradient over each surface, grouping positive and negative gradients separately, and thereby locating the adiabatic contour. The Nusselt number was thus defined by

$$Nu = \dot{Q}L/Ak(T_{\mathrm{H}} - T_{\mathrm{C}}),$$

where k is the thermal conductivity of the filling, T_{H} and T_{C} are the hotter and cooler end temperatures, respectively, and $A = D^2 + 2LD$ is half the total surface area of the cavity. Using grids of $11 \times 11 \times 51$, $13 \times 13 \times 61$ and $15 \times 15 \times 71$, a comparison of Nusselt number was made for $Ra = 5 \times 10^3$, 2.5×10^4, 10^5 and 10^6. For each Rayleigh number, the spread in the Nusselt number was found to be less than 5%. In addition, the programme was checked against the data of Mallinson & de Vahl Davis (1977) for a shorter rectangular cavity. Agreement better than 2% was obtained for the Nusselt numbers.

In the lower range, it is apparent that a conduction regime persists up to $Ra = O(10^{2.5})$ at which point advection becomes important. The flow system for higher Rayleigh numbers has been studied by Bontoux *et al.* (1986*c*). Just beyond the conduction regime, the heat transfer curve is seen to be concave up, a feature which continues up to a point of inflection in the neighbourhood of $Ra = 10^{3.5}$. Bontoux *et al.* (1986*c*) suggested a transition at $Ra = 2.21 \times 10^4$ from a 'core-driven' regime, but this appears to have no particular significance in heat transfer terms. How far beyond the point of inflection downward concavity persists is unknown, but it is not unreasonable to assume a behaviour analogous to that observed in the vertical thermosyphon.

As noted by Bayley & Lock (1965), the laminar boundary layer regime for a vertical tube in which the boundary-layer thickness δ is given by

$$\frac{\delta}{D} \sim \left(\frac{S}{Ra}\right)^{\frac{1}{4}},$$

persists to $Ra/S = O(10^5)$: that is, until $\delta = O(D/18)$, which, although a small fraction, corresponds to the core velocity reaching about one-fifth of the boundary-

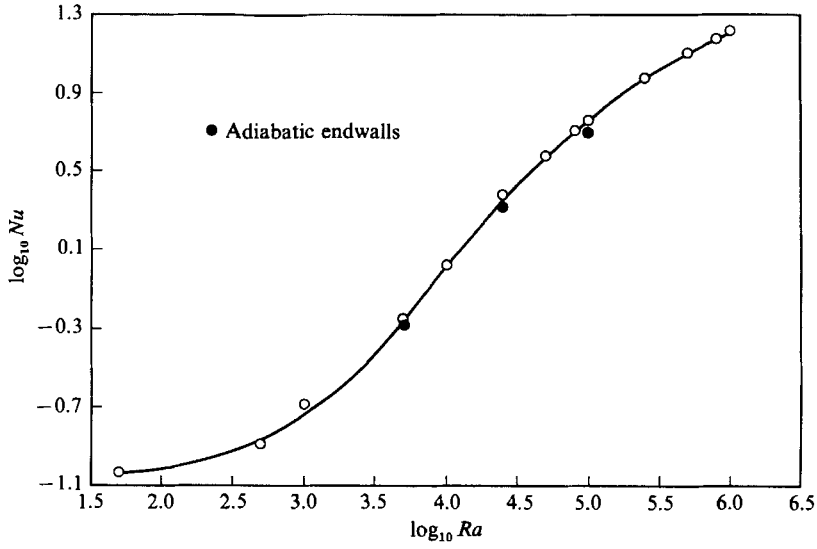

FIGURE 2. Overall Nusselt number as a function of Rayleigh number: $S = 5$.

layer velocity. Below this value of Ra/S, a thicker boundary layer is more strongly opposed by the core flow in what has been called the impeded regime (see Lighthill 1953). In a horizontal cavity lying parallel to the ambient temperature gradient the flow is driven both by direct buoyancy effects, manifest near the side- and endwalls, and by indirect buoyancy effects attributable to the horizontal temperature (pressure) gradient. If the latter effect were the weaker, it would be natural to use the parameter Ra/S to define the flow regimes, but for horizontal cavities with a large slenderness ratio such an approach would seem to be less appropriate. Assuming instead that indirect buoyancy effects dominate (as might be expected, for example, if the slenderness ratio were especially large and the end faces were adiabatic), the same scaling procedure which led to the group Ra/S for the vertical cavity leads to Ra/S^2 for the horizontal cavity: that is

$$\frac{\delta}{D} \sim \left(\frac{S^2}{Ra}\right)^{\frac{1}{5}}$$

in which the $\frac{1}{5}$th power replaces the $\frac{1}{4}$th power appropriate only to a vertical surface. If it is again assumed that the boundary-layer regime ends when $\delta = O(D/18)$ it follows that the transition would occur when $Ra/S^2 = O(18 \times 10^5)$, or, for $S = 5$, when $Ra = O(10^7)$. This magnitude is beyond the range of the data in figure 2, but given the likelihood that direct buoyancy was not unimportant it is not inconsistent with the suggestion that true boundary-layer flow did not exist below $Ra = 10^5$, and possibly not below $Ra = 10^6$. In other words, the range $2.5 \lesssim \log_{10} Ra \lesssim 6$ might be appropriately described as an impeded regime. In such a regime, a simple heat balance implies that $Nu \sim Ra/S^2$. A slope of unity occurs in the vicinity of $Ra = 10^{3.8}$, but the intersection of the tangents from that point and from the anticipated boundary-layer regime (where the slope is 0.2) indicate that the transition between the regimes extends over two orders of magnitude in the Rayleigh number. A similar comment applies to the lower transition. The impeded regime is therefore never well established, and acts more like an extended transition between the conduction and boundary-layer regimes.

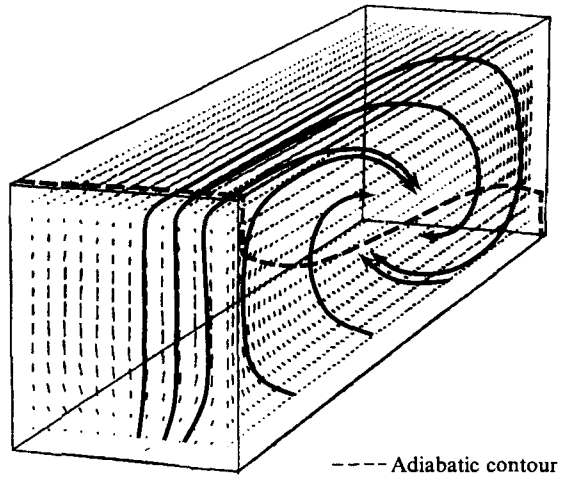

FIGURE 3. Peripheral flow in a horizontal cavity: $Ra = 2.5 \times 10^4$.

The 'peripheral' flow in the annular region near the cavity walls when $Ra = 2.5 \times 10^4$ is shown in figure 3 which was obtained by first erecting the velocity vectors at nodal points in planes which were one grid point in from the cavity surface, and then constructing curves with the vectors as tangents. The 'streamlines' thus formed suggest the outer flow pattern which would be seen by an observer looking through transparent walls at dye injected through the walls. This is the flow which occurs close to the 'transitional' value of Ra suggested by Bontoux *et al.* (1986*c*), and has the same form as that observed by those workers.

Figure 3 also shows the adiabatic contour (dashed) on the surface of the cavity for $Ra = 2.4 \times 10^5$ and figure 4 details the heat transfer contributions attributable to each of the five faces over which heat enters the fluid: the heat leaving the fluid over the remaining surface areas (half the total) must balance this heat addition. It is evident that most of the heat transfer occurs over the bottom surface area which is the greatest (see figure 3) and is associated with eversion: that is, the fluid of the lower half of the core turns inside out as it moves towards the hotter end; the coldest (inner) region of the core descends towards the bottom surface of the cavity, is warmed by passage over the bottom and sides, and then returns to the core. Obviously, the same mechanism, augmenting heat loss, operates in the hotter fluid of the upper half of the core moving in the opposite direction, and the two subsystems interface over a surface, the perimeter of which is suggested in figure 3. It is of interest to note that the contribution of the end face is only about 10% of the total heat transfer rate. This order of magnitude is reflected in the discrete points plotted in figure 2; these were obtained in precisely the same way but with an imposed adiabatic end-wall condition. Clearly, the neglect of endwall heat transfer would be unacceptable for the configuration given; diffusion and advection are not unimportant in the end regions. However, it is not unreasonable to expect that the relative contribution of the ends would decrease as the slenderness ratio increased to the point where Ra/S^2, with its emphasis on indirect buoyancy effects, would be a better correlating variable than Ra/S.

The internal details of the flow are revealed in figures 5, 6 and 7 the first of which shows the axial velocity profile at three transverse sections in the hotter half of the tube. As anticipated, axial motion is limited near the endwall but rapidly increases

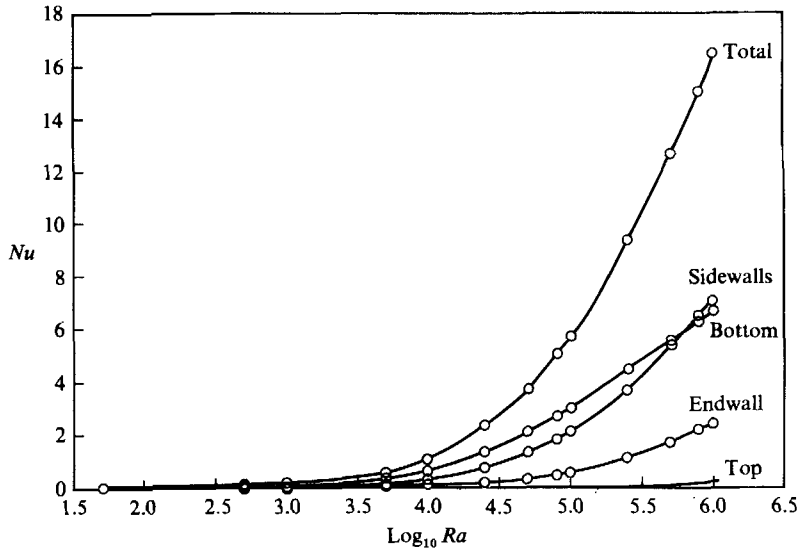

FIGURE 4. Components of the heat transfer rate.

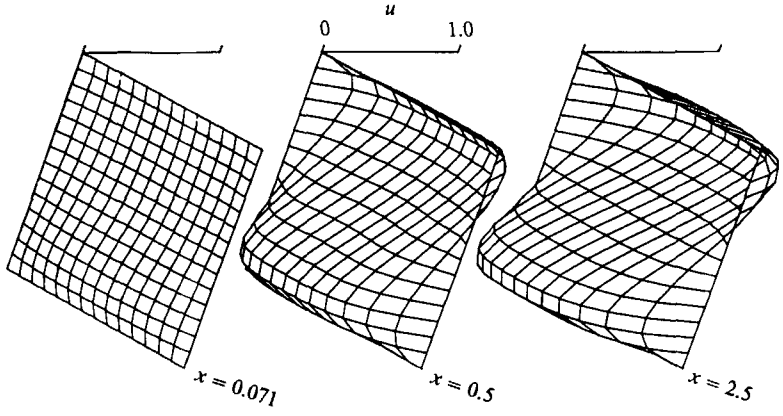

FIGURE 5. Axial velocity profiles in a horizontal cavity: $Ra = 2.5 \times 10^4$.

over a distance comparable with half of the cavity width, thereafter varying more slowly in the 'core' of the cavity. It is evident that over most of the cavity length the flow is almost parallel. Apart from the effect of the sidewalls, the general form of the velocity profile is the familiar S-shape of the infinitely wide cavity so extensively studied. Figure 6 amplifies the structural details by showing how vertical velocity changes occur in the vicinity of the end- and sidewalls. The figure confirms that the end region extends over only about one half of the cavity width at this Rayleigh number but its effect is merged with that of the sidewalls. This latter effect evidently extends over the entire length of the cavity and penetrates almost to the longitudinal axis. It is therefore difficult to imagine this system as a true boundary-layer flow. Figures 5, 6 and 7 reveal the same general circulation pattern as that obtained for a circular cylinder (Bontoux *et al.* 1986*c*).

Some of the data implicit in figure 6 have been used in figure 7 to construct the transverse flow field at several distances from the hotter end. Various flow zones are

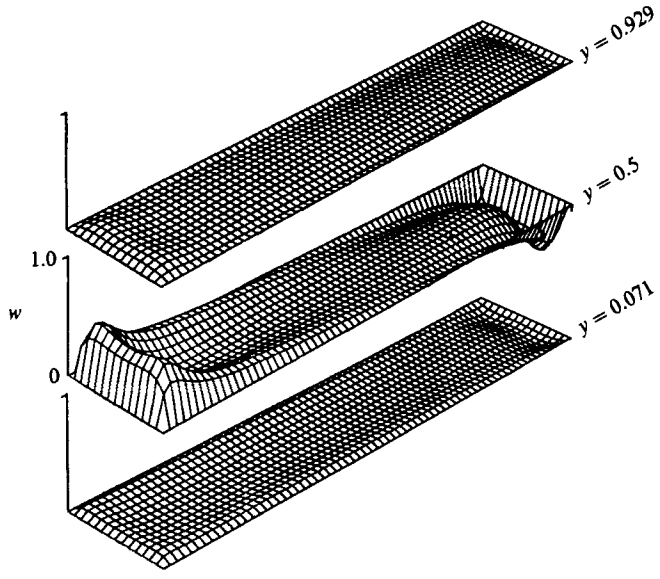

FIGURE 6. Vertical velocity profiles: $Ra = 2.5 \times 10^4$.

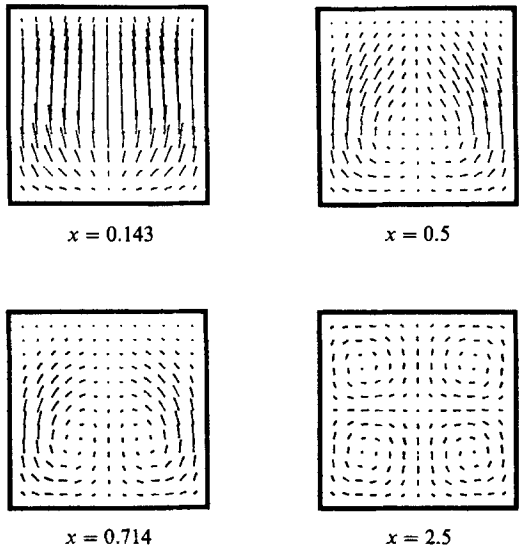

FIGURE 7. Transverse velocity field in a horizontal cavity: $Ra = 2.5 \times 10^4$.

evident. Near the endwall the direct effect of buoyancy is dominant, while far from the wall the vortex pairs are evident in an eversion zone, culminating in the doubly symmetric flow field of the central lateral plane. Between the end zone and the eversion zone is a small transitional zone ($x \approx 0.5$) containing the outer edge of the vortex loop indicated in figure 6. Corresponding to these velocity profiles are the temperature profiles of figure 8, which makes clear the connection between the zones: the profiles are measured relative to the local wall temperature. Near the end of the cavity, the bulk of the cooler fluid is situated in the lower half, and the lateral temperature gradient at the top and neighbouring sides of the cavity is almost zero.

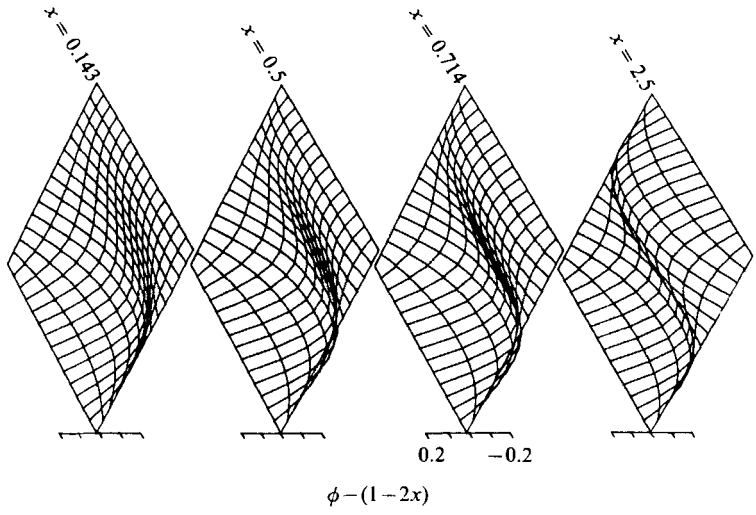

FIGURE 8. Transverse temperature profiles: $Ra = 2.5 \times 10^4$.

However, as we proceed towards the central lateral plane the lateral temperature gradient over the top surface and the upper half of the sides increases steadily. The effect of this is to create in the upper half of the cavity the vortical eversion detailed in figure 7.

3.2. *The effect of inclination*

The effect of inclination on heat transfer may be seen in figure 9 which was obtained with $Ra = 2.5 \times 1.0^4$. As anticipated, the overall Nusselt number increases with inclination above the horizontal and decreases with inclination below, but the precise shape of the curve deserves closer attention. For inclinations which are negative the dependency was found to be a monotonic function, concave up. The basic circulation associated with the horizontal position persists with reduced velocities, and as $\alpha \to -90°$ heat transfer tends towards pure conduction through the then quiescent air filling. This is a one-dimensional situation demanding congruence with the three-dimensional prediction and a two-dimensional prediction (shown dashed) obtained for the same volume of air with sidewall boundary conditions replaced by $\phi_y = u_y = w_y = v = 0$. In general the effect of the sidewalls is two-fold: lateral conduction promotes secondary circulation, increasing heat transfer, while viscous drag reduces heat transfer. The two-dimensional curve in figure 9 thus indicates the relative importance of these opposing effects.

It is evident that when $Ra > 10^{2.5}$, the vortex-pair flow model discussed above adequately describes convection within the cavity for inclinations in the range $-180° \leqslant \alpha \leqslant 0$. However, increased heat transfer produced by rotation of the cavity above (or below) $\alpha = -90°$ is evidently attributable to increased primary circulation: that is, the vortex pairs facilitate only a small advective exchange, the effect of which increases slightly with increases in the indirect buoyancy effects.

The flow system is modified when α increases above zero. As the upper full curve in figure 9 indicates, the smooth, concave shape is interrupted not far from the horizontal position at an inclination which appears to separate two concave sections of the curve, the second extending from $\alpha \approx 5°$ up to $\alpha \approx 30°$. Figure 10 shows the peripheral flow when $\alpha = 30°$, for which a recirculating end flow is evident. The cause of the latter becomes clear from figure 11 which displays the transverse velocity field

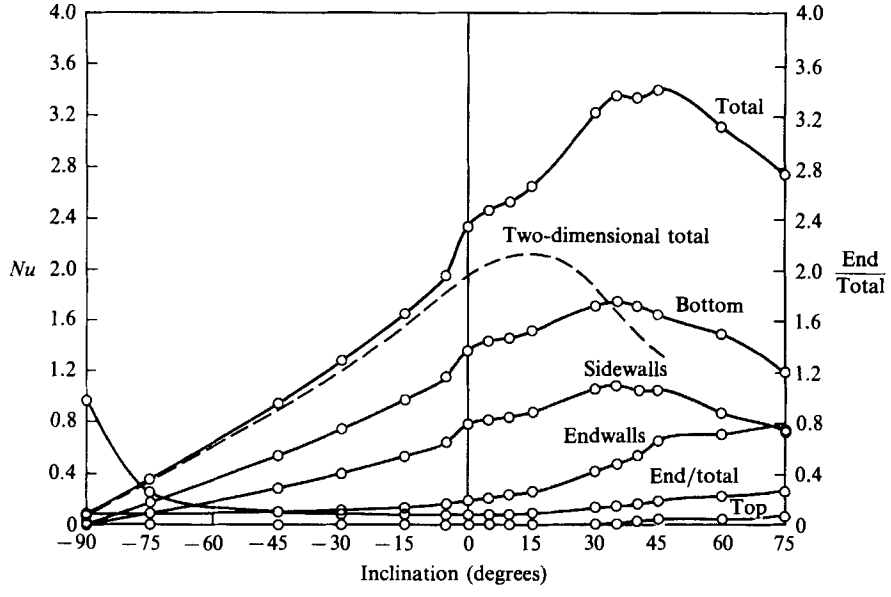

FIGURE 9. The effect of inclination on heat transfer.

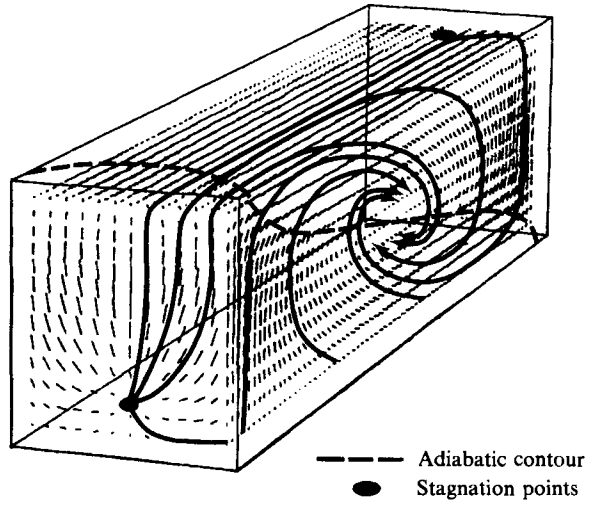

FIGURE 10. Peripheral flow with 30° inclination: $Ra = 2.5 \times 10^4$.

near the cooler end. Gradual tilting of the cavity above the horizontal has evidently increased the axial velocity of the upper (hotter) section of the core while increasing the direct buoyancy force opposing it near the cavity top; at the same time, the downward direct effect of buoyancy near the endwall is reduced. Eventually, the inertia of the core, aided by these modifications in the buoyancy forces in the top corner of the cavity, creates a stagnation point on the endwall, thus requiring the core to split. This behaviour was also found in the two-dimensional cavity and has been observed by Bontoux *et al.* (1986*b*) in a circular cylinder.

The effect of the end stagnation points is to make possible more vigorous convection in the end regions, the central region remaining essentially unchanged, at

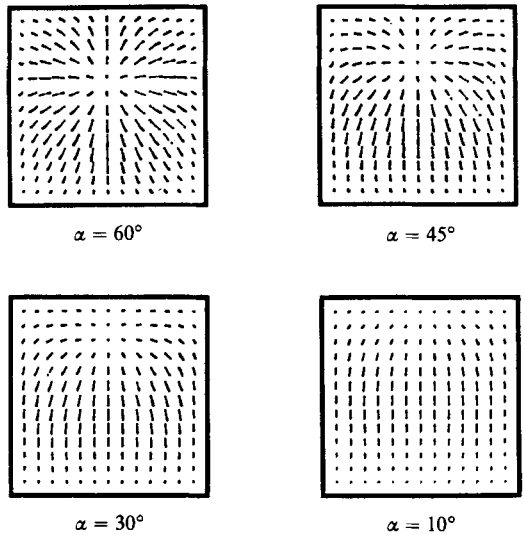

FIGURE 11. Cold-end velocity field of inclined cavity: $Ra = 2.5 \times 10^4$.

least from the point of view of flow structure. Heat transfer through the cavity thus continues to be principally by advective exchange. In the three-dimensional cavity, such modified vortical advective behaviour is reflected in the upper concavity for $0 < \alpha < 30°$, as indicated in the Nu–α curve shown in figure 9. However, before the system shifts to modified vortical advection, the opposing effects of inertia and buoyancy near $\alpha = 0°$ must pass through a point of balance when circulation in the highest and lowest corners of the cavity will be reduced to a minimum. The corresponding hesitation in the Nu–α curve with $Ra = 2.5 \times 10^4$ extends over a very small range of inclinations centred near $\alpha = 5°$, when the endwall stagnation points were first detected in the finite cavity.

It is to be expected that modified vortical advection would continue with increasing inclination so long as the lateral component of the gravitational acceleration is sufficient to drive it, but this induced flow is organized by the sidewalls which must also propagate the opposing effect of an increase in the longitudinal component of the same body force field. For $Ra = 2.5 \times 10^4$, the relative importance of these two components evidently undergoes a significant shift near $\alpha = 45°$, as figure 9 indicates. Beyond this inclination, the secondary flow gradually subsides, a feature noted in the work of Bontoux *et al.* (1986*b*). This is a crucial transition because the heat transfer efficiency of the system is impaired accordingly. As inclination increases above $\alpha = 5°$, the end stagnation points move closer to the centre of the end faces, as illustrated in figure 11. This has the eventual effect of changing the flow in the end regions from the simple 180° change in direction associated with a two-filament core to one in which a more centrally located (though still displaced) core is surrounded by an annulus of fluid moving away from the end. The alteration evidently takes places gradually between $\alpha = 5°$ and $\alpha = 45°$.

In contrast, the two-dimensional result reveals a maximum heat transfer rate near $\alpha = 15°$ with a fairly rapid decline thereafter. It is thus evident that secondary motion has a substantial effect on heat transfer in the range $0 < \alpha < 45°$. Above this range the solution was found to be intrinsically three-dimensional despite the application of two-dimensional boundary conditions; comparison with a two-dimensional flow is no longer meaningful.

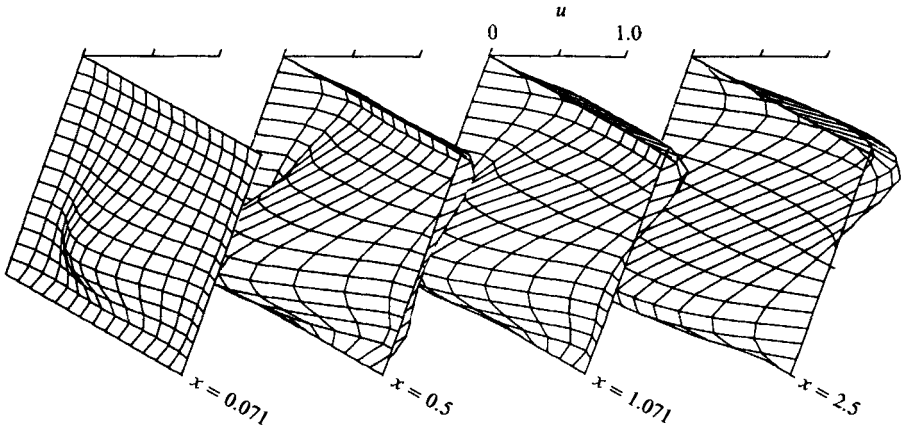

FIGURE 12. Axial velocity profiles in an inclined cavity: $\alpha = 60°$, $Ra = 2.5 \times 10^4$.

Despite the modification of the end region flow, the main pattern in the finite cavity still consists of two filaments moving in opposite directions, each filament reaching the endwall in the vicinity of the stagnation point. The principal thermal exchange mechanism between the hotter and cooler ends continues to be advection and the peripheral flow pattern is qualitatively similar to that shown in figure 10. However, the velocity field in transverse planes for $\alpha > 45°$ revealed no evidence of the vortex pairs so characteristic of the flow when $\alpha \leqslant 45°$. The axial velocity profiles shown in figure 12 illustrate how the refluent end flow is transformed into the central two-filament flow within about one cavity width from the end.

If this flow pattern modification were to continue through to the vertical position, it might be expected that the stagnation points on the top and bottom walls would approach closer to, and eventually reach, the central lateral plane. However, the antisymmetry of the opposed filaments would be at odds with the symmetry one would expect about the central lateral plane when the cavity was vertical. The behaviour of the system in the vertical position is currently the subject of further study, but for present purposes perhaps a few general observations may be useful. Of the thermal exchange mechanisms suggested by Bayley & Lock (1965), advection and refluence represent the optimum and pessimum, respectively. The continuation of an advection mechanism for $45° < \alpha \leqslant 90°$ would lead to a Nusselt number increasing with inclination, presumably monotonically. But figure 9 shows that while the decaying effect of eversion leads to maxima in side and bottom wall heat transfer rates at $\alpha \approx 35°$, the overall heat transfer rate reaches a local maximum first at $\alpha = 35°$ and again at $\alpha = 45°$, the bimodality being caused by direct buoyancy effects in the end region. It is clear from figure 9 that this trend is not continued in the end region and the overall heat transfer rate therefore falls for α beyond 45°.

It is suggested that changes in circulation pattern do in fact occur near $\alpha \to 90°$. One possibility is that the two-filament advective pattern is replaced by an advective core–annulus pattern in which some form of interdigitative cross-over occurs in the vicinity of the central lateral plane. If so, the small increases in direct buoyancy effects as $\alpha \to 90°$ would likely be offset by small increases in circulation resistance attributable to the advective coupling: that is, the overall heat transfer rate would not be expected to change significantly in the range $45° < \alpha < 90°$. This conclusion is not supported by figure 9. Alternatively, the two-filament model may be replaced by a core–annulus model in which no mass is transferred across the central lateral

plane: that is, the central flow field, like the endflow, is completely refluent. If so, a dramatic reduction in heat transfer would follow because it would consist of pure conduction across an area equal to the cross-sectional area of the cavity. Although an hypothesis, this suggestion is consistent with the falling heat transfer rate evident in figure 9 between $\alpha = 45°$ and $\alpha = 90°$.

4. Conclusions

Buoyant, laminar convection in a long, square-section cavity has been studied numerically for situations in which the ambient temperature gradient is parallel to the longitudinal axis of the cavity. Internal details of the flow system in a cavity with a slenderness ratio of 5:1 have been used to develop a global flow model, the changing structure of which has been correlated with the overall rate of heat transfer into, through, and out of the system. Several flow regimes have been identified, enabling comparisons to be made with previous work.

In the horizontal position, heat transfer was limited to longitudinal conduction for $Ra \leqslant 10^{2.5}$. Fluid motion then consisted of a single circulating loop: a core of two opposed filaments and two end regions in which the flow simply doubled back. Above this Rayleigh number, each core filament developed a secondary motion in the form of a vortex pair, the lateral extent of which increased in the direction of filament motion. Such evertive behaviour was found to produce a significant increase in heat transfer rate. This form of vortical advection between the hotter and cooler ends continued with increasing Rayleigh number, at least up to $Ra = 10^6$. The internal details of the flow at $Ra = 2.5 \times 10^4$ are quite similar to those reported for a circular cylinder by Bontoux *et al.* but no evidence of boundary-layer conditions was found. As a result of comparison with the analogous behaviour of the closed tube vertical thermosyphon, it is suggested that a true boundary-layer regime does not exist below $Ra = 10^6$ for this particular geometry. Consequently the range $O(10^{2.5}) < Ra < O(10^6)$ has been described as an impeded regime.

Inclinations of the cavity below the horizontal (the hotter end being higher) generated no change in fundamental flow behaviour for $Ra = 2.5 \times 10^4$. There appears to be no reason why the behaviour would be modified by lower values of Ra, or indeed by higher values under laminar conditions. Positive inclinations, however, did produce substantial changes in behaviour. In the vicinity of $\alpha = 5°$, stagnation points appeared on the endwalls, gradually moving along the wall from the corners of the cavity towards the longitudinal axis as the inclination increased. This change marked the onset of a split end flow as opposed to a single 180° turn, and thus led to refluence in the upper and lower corners of the cavity. These modifications in the end regions were detected on the heat transfer curve but changed only slightly between $\alpha = 5°$ and 45°, at which point the secondary vortical flow had been reduced to negligible proportions. The basic features of the speculative flow model discussed by Lock & Kirchner – namely, two opposed filaments in which eversion is operative – were confirmed.

Beyond $\alpha = 45°$ the heat transfer rate declined noticeably. This has been attributed to the absence of eversion and increasing proximity to a vertical flow pattern characterized by complete refluence in the central region of the cavity. Under such conditions, heat transfer between the hotter and cooler ends would gradually be reduced to pure conduction over the central cross-sectional area of the cavity. The behaviour of the vertical system is to be reported in a companion paper.

This work was begun with a grant under the Alberta Municipal Affairs Innovative Housing Programme and was completed with assistance from the Natural Sciences and Engineering Research Council of Canada. We wish to record our gratitude to both of these organizations, and to the anonymous reviewers whose comments led to several improvements.

REFERENCES

BAYLEY, F. J. & LOCK, G. S. H. 1965 Heat transfer characteristics of the closed thermosyphon. *Trans. ASME* C: *J. Heat Transfer* **87**, 30–40.

BEJAN, A., AL-HOMOUD, A. A. & IMBERGER, J. 1981 Experimental study of high-Rayleigh-number convection in a horizontal cavity with different end temperatures. *J. Fluid Mech.* **109**, 283–299.

BEJAN, A. & TIEN, C. L. 1978*a* Laminar natural convection heat transfer in a horizontal cavity with different end temperatures. *Trans. ASME* C: *J. Heat Transfer* **100**, 641–647.

BEJAN, A. & TIEN, C. L. 1978*b* Fully developed counterflow in a long horizontal pipe with different end temperatures. *Intl J. Heat Mass Transfer* **21**, 701–708.

BLYTHE, P. A., DANIELS, P. G. & SIMPKINS, P. G. 1983 Thermal convection in a cavity: the core structure near the horizontal boundaries. *Proc. R. Soc. Lond.* A **387**, 367–388.

BONTOUX, P., ROUX, B., SCHIROKY, G. H., MARKHAM, B. L. & ROSENBERGER, F. 1986*a* Convection in the vertical midplane of a horizontal cylinder. Comparison of two-dimensional approximations with three-dimensional results. *Intl. J. Heat Mass Transfer* **29**, 227–239.

BONTOUX, P., SMUTEK, C., RANDRIAMAMPIANINA, A., ROUX, B., EXTREMET, G. P., HURFORD, A. C., ROSENBERGER, F. & VAHL DAVIS, G. DE 1986*b* Numerical solutions and experimental results for three-dimensional buoyancy driven flows in tilted cylinders. *Adv. Space Res.* **6**, 155–160.

BONTOUX, P., SMUTEK, C., ROUX, B. & LACROIX, J. M. 1986*c* Three-dimensional buoyancy-driven flows in cylindrical cavities with differentially heated endwalls. Part 1. Horizontal cylinders. *J. Fluid Mech.* **169**, 211–227.

CORMACK, D. E., LEAL, L. G. & IMBERGER, J. 1974*b* Natural convection in a shallow cavity with differentially heated endwalls. Part 1. Asymptotic theory. *J. Fluid Mech.* **65**, 209–229.

CORMACK, D. E., LEAL, L. G. & SEINFIELD, J. N. 1974*b* Natural convection in a shallow cavity with differentially heated endwalls. Part 2. Numerical solutions. *J. Fluid Mech.* **65**, 231–246.

IMBERGER, J. 1974 Natural convection in a shallow cavity with differentially heated endwalls. Part 3. Experimental results. *J. Fluid Mech.* **65**, 2247–2260.

JAPIKSE, D. & WINTER, E. R. F. 1971 Heat transfer and fluid flow in the closed thermosyphon. *Intl J. Heat Mass Transfer* **14**, 427–441.

LIGHTHILL, M. J. 1953 Theoretical considerations on free convection in tubes. *Q. J. Mech. Appl. Maths.* **6**, 398–439.

LOCK, G. S. H. & KIRCHNER, J. D. 1988 Flow and heat transfer in an inclined, closed tube thermosyphon. In: *Proc. 27th Natl H.T. Conf.* ASME.

MALLINSON, G. D. & VAHL DAVIS, G. DE 1977 Three-dimensional natural convection in a box: a numerical study. *J. Fluid Mech.* **83**, 1–31.

MENOLD, E. R. & OSTRACH, S. 1965 Natural convection in a horizontal cylinder at large Prandtl numbers. *Case Inst. of Technol. SFOSR Tech. Rep.* 65–2239.

OSTRACH, S. 1972 Natural convection in enclosures. *Adv. Heat Transfer* **8**, 161–227.

OSTRACH, S., LOKA, R. R. & KUMAR, A. 1980 Natural convection in low aspect ratio rectangular enclosures. In *Natural Convection in Enclosures*, HTD-8, pp. 1–10. ASME.

PATANKAR, S. V. 1981 A calculation procedure for two dimensional elliptic equations. *Numer. Heat Transfer* **4**, 409–425.

SABZEVARI, A. & OSTRACH, S. 1966 Experimental studies of natural convection in a horizontal cylinder. *Case Inst. of Technol. AFOSR Tech. Rep.* 66–1401.

SCHIROKY, G. H. & ROSENBERGER, F. 1984 Free convection of gases in a horizontal cylinder with differentially heated endwalls. *Intl. J. Heat Mass Transfer* **27**, 587–598.

SIMPKINS, P. G. & CHEN, K. S. 1986 Convection in horizontal cavities. *J. Fluid Mech.* **166**, 21–39.

SMUTEK, C., BONTOUX, P., ROUX, B., SCHIROKY, G. H., HURFORD, A., ROSENBERGER, F. & VAHL DAVIS, G. DE 1985 Three-dimensional convection in horizontal cylinders – numerical solutions and comparison with experimenta and analytical results. *Numer. Heat Transfer* **8**, 613–631.

VAN DOORMAAL, J. P. & RAITHBY, G. D. 1984 Enhancements of the SIMPLE method for predicting incompressible fluid flows. *Numer. Heat Transfer* **7**, 147–163.